Available online at www.sciencedirect.com
SCIENCE DIRECT
Sensors and Actuators A 109 (2003) 102–113
SENSORS AND ACTUATORS A PHYSICAL
www.elsevier.com/locate/sna

Low-cost uncooled infrared detectors in CMOS process

Selim Eminoglu, Deniz Sabuncuoglu Tezcan, M. Yusuf Tanrikulu, Tayfun Akin*

Department of Electrical and Electronics Engineering, Middle East Technical University, Ankara 06531, Turkey

Received 19 November 2002; received in revised form 5 August 2003; accepted 20 August 2003

Abstract

This paper reports the implementation and comparison of two low-cost uncooled infrared microbolometer detectors that can be implemented using standard n-well CMOS processes. One type is based on a suspended n-well resistor, which is implemented in a 0.8 μm CMOS process and has a pixel size of 80 μm × 80 μm with a fill factor of 13%; and the other type is based on a suspended p^+-active/n-well diode, which is implemented in a 0.35 μm CMOS process and has a pixel size of 40 μm × 40 μm with a fill factor of 44%. These detectors can be obtained with simple bulk-micromachining processes after the CMOS fabrication, without the need for any complicated lithography or deposition steps. The diode type detector has a measured dc responsivity ($\Re$) of 4970 V/W at 20 μA bias and a thermal time constant of 35.8 ms at 80 mTorr vacuum level, and it has a measured rms noise of 0.52 μV for a 4 kHz bandwidth, resulting in a detectivity (D^*) of 9.7×10^8 cm Hz$^{1/2}$/W. The resistive n-well detector can provide the same dc responsivity at 1.68 V detector bias voltage, with about 10 times more self-heating as compared to that of the diode type detector. This detector has a measured rms noise of 0.81 μV for a 4 kHz bandwidth, resulting in a detectivity (D^*) of 8.9×10^8 cm Hz$^{1/2}$/W, which can be improved further with higher detector bias voltages at the expense of increased self-heating. The diode type detector is better for low-cost large format infrared detector arrays, since it has a superior response even at reduced pixel sizes and lower biasing levels.
© 2003 Elsevier B.V. All rights reserved.

Keywords: Uncooled infrared detector; CMOS infrared detector; Microbolometer; Low-cost infrared detector; IR detector; CMOS micromachined sensor

1. Introduction

Uncooled infrared detectors have recently gained wide attention for infrared imaging applications, due to their advantages such as low cost, low weight, low power, wide spectral response, and long-term operation compared to those of photon detectors. Worldwide effort is still continuing to implement very large format arrays at low cost for use in various applications, including commercial applications like driver's night vision enhancement and fire fighting. One of the main issues for achieving low-cost detectors is their monolithic integration and compatibility with CMOS technology.

The most widely used uncooled detector approach is to implement microbolometers using surface micromachined bridges on CMOS processed wafers, where infrared radiation increases the temperature of a material formed on the thermally isolated and suspended bridge, causing a change in its resistance related to its temperature coefficient of resistance (TCR) [1–9]. Currently, there are microbolometer arrays with 640 × 480 array formats and 25 μm × 25 μm pixel sizes with performance approaching that of cooled photon detectors [1]. However, these detectors require deposition of some high TCR materials after CMOS fabrication and complicated post-CMOS surface micromachining processing, increasing its cost and limiting its use for ultra low-cost commercial applications. For example, vanadium oxide (VO_x), which is the most widely known and used microbolometer material, has a high TCR of about 2–3%/K [2]; however, VO_x is not a standard material in IC fabrication and requires dedicated expensive equipment to prevent contamination of the CMOS line. In addition, it exhibits large $1/f$ noise due to its non-crystalline structure. There are efforts to implement surface micromachined microbolometers using IC compatible materials such as amorphous silicon [3], amorphous silicon carbide [4], and polycrystalline silicon–germanium [5]; and these materials also have high TCR values of 2.5, 4–6, and 2–3%/K, respectively. However, these materials require high temperature annealing to reduce their residual stress, which is not suitable for post-CMOS processing for monolithic integration. In addition, they exhibit even higher $1/f$ noise than VO_x, due to their non-crystalline structures. Another high TCR microbolometer material that is recently used is YBaCuO, which is deposited at room temperature, however, these detectors still require complicated and

* Corresponding author. Tel.: +90-312-210-2369;
fax: +90-312-210-1261.
E-mail address: tayfun-akin@metu.edu.tr (T. Akin).

0924-4247/$ – see front matter © 2003 Elsevier B.V. All rights reserved.
doi:10.1016/j.sna.2003.08.013

expensive post-CMOS surface micromachining processes [6,7]. There are also microbolometers implemented with IC compatible metal films [8,9], however, these detectors still require deposition and lithography steps after CMOS, and their performances are low due to low TCR of metal films. Therefore, although surface micromachined microbolometers are very cheap compared to photon detectors, their price is still high for many commercial applications due to extra processes required for their fabrication.

Low-cost infrared detectors can be implemented with front or back-end bulk-micromachining of CMOS fabricated wafers, and this approach has mostly been used to implement CMOS thermopile arrays [10,11]. However, thermopile arrays have low responsivity values (5–15 V/W) and large pixel sizes (250 μm × 250 μm), limiting their use for large detector arrays. In addition, these detectors also require extra processing steps to form silicon islands [10] or electroplated gold lines [11] for thermal isolation between the pixels when back-end bulk-micromachining is used.

Recently, a new bulk-micromachining approach has been emerged, where forward biased silicon p–n diodes are used as uncooled infrared detectors. Up to now, two such approaches have been reported. One of them uses a suspended single p–n diode implemented using a dedicated in-house process technology [12], however, this approach does not seem suitable for large format arrays, due to its large pixel size of 100 μm × 170 μm [13]. The other diode microbolometer approach uses suspended multiple series diodes with 40 μm × 40 μm pixel sizes implemented in a SOI CMOS process [14]. Although this approach has very good potential for low-cost high-performance uncooled detectors and successful implementation of a 320 × 240 FPA has been reported, the fabrication is based on a dedicated in-house SOI process, limiting its cost reduction. For ultra low-cost applications, the best approach would be to implement the detector arrays together with their readout circuitry fully in a standard CMOS process, using some simple post-CMOS etching steps where neither lithography nor detector material deposition is needed.

This paper reports the implementation and comparison of two kinds of such ultra low-cost bulk-micromachined uncooled microbolometers that can be implemented using standard n-well CMOS processes [15]: one is based on suspended n-well resistor, and the other is based on suspended p^+-active/n-well diode. Suspended n-well structures are obtained by post-CMOS anisotropic silicon etching. Since this fabrication approach does not require any lithography or advanced detector material deposition, the detector cost is almost equal to the CMOS chip cost. We have previously reported the development of low-cost uncooled resistive microbolometer detector arrays with 16 × 16 array sizes, where the pixel size was 80 μm × 80 μm with a fill factor of only 13% [16–18]. Recently, we have developed a new detector with much smaller pixel size and higher fill factor to implement larger FPAs with higher performance [15,19]. In this approach, a diode type pixel with 40 μm × 40 μm pixel size and a fill factor of 44% is used. This paper reports the comparison of these two CMOS compatible uncooled infrared detectors and their feasibility to implement large FPAs.

2. Pixel structure and fabrication

Fig. 1 shows the perspective view of the low-cost uncooled infrared detector that can be implemented with simple etching steps after CMOS fabrication. This structure can be used to implement both resistive and diode type microbolometers. Since this structure can be obtained without any complicated lithography or deposition step, the cost of the detectors is very low. Fig. 2(a) shows the post-processing steps of resistive type n-well microbolometer. The n-well layer is surrounded by an opening area that allows silicon underneath to be exposed for etching from the front side of the wafer without the need for any lithography step. The required openings for etching is formed by placing the various openings in the CMOS layers on top of each other during the design, including active, contact, via, and passivation openings [20]. After the CMOS fabrication process, the electrochemical etch-stop technique in TMAH is used to thermally isolate the n-wells from the substrate, as described previously [21]. The resistive type structures with 80 μm × 80 μm pixel size were implemented in a 0.8 μm process, where only simple

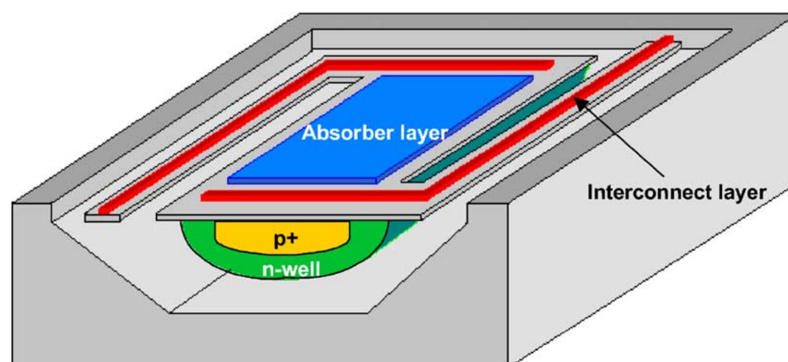

Fig. 1. The perspective view of the low-cost uncooled infrared detector that can be implemented with simple etching steps after CMOS fabrication.

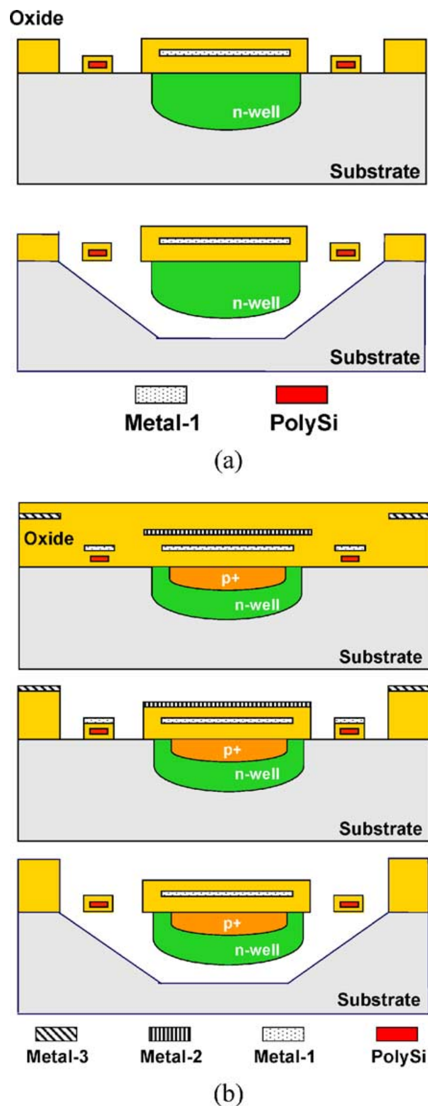

Fig. 2. The post-processing steps of (a) resistive type and (b) diode type n-well microbolometers.

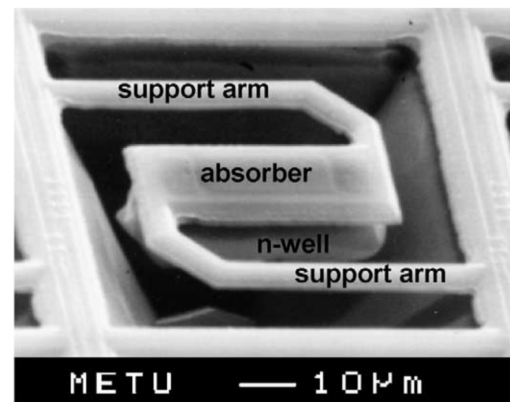

(a)

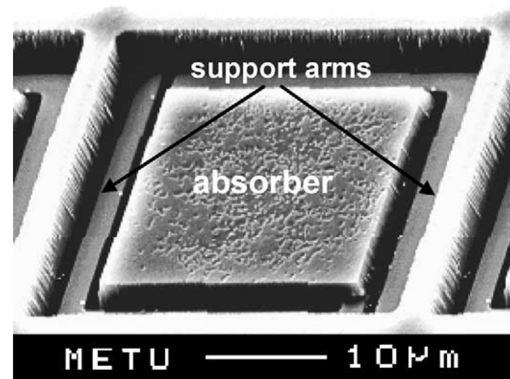

(b)

Fig. 3. SEM photographs of the fabricated microbolometers: (a) resistive type with an 80 µm × 80 µm pixel size and a 13% fill factor implemented in a 0.8 µm CMOS process and (b) diode type with a 40 µm × 40 µm pixel size with a 44% fill factor implemented in a 0.35 µm CMOS process.

wet etching is enough for post-CMOS processing at the expense of larger pixel size and smaller fill factor (13%). The infrared absorber layer of the structure is implemented using dielectric and metal sandwiches that are readily available in standard CMOS for low cost. This type of absorber layers can provide absorption coefficient values between 0.30 and 0.75, depending on the type and number of these layers [22].

The diode type detector is implemented using a sub-micron CMOS technology with a new post-CMOS etching process to decrease the pixel size down to 40 µm × 40 µm and to increase the fill factor up to 44%. Fig. 2(b) shows post-processing steps of diode type microbolometers where an additional RIE (reactive ion etching) step is included before the bulk-micromachining. In RIE, CMOS metal layers are used as etch-masks to eliminate any critical lithography step after CMOS [23] while achieving narrow etch openings of about 1.2 µm between the support arms. After RIE, masking metal layers are removed, and then, the bulk silicon underneath the detector is etched while protecting the n-well layer using an electrochemical etch-stop technique in TMAH. Fig. 3(a) and (b) show the SEM photographs of the fabricated resistive and diode type microbolometers in two different CMOS processes, respectively. Fig. 4 shows the SEM photograph of the diode type detector taken looking from the backside, where the suspended n-well is clearly visible. This photograph is taken after separating the pixel from the substrate using a sticky-tape.

3. Measurement results and comparison

A number of measurements and simulations have been performed to determine and compare the performance of the resistive and diode type microbolometer detectors. The performance parameters used in comparison include their pixel size, thermal conductance values, pixel TCR and temperature coefficient of the pixel voltage, responsivity, electrical

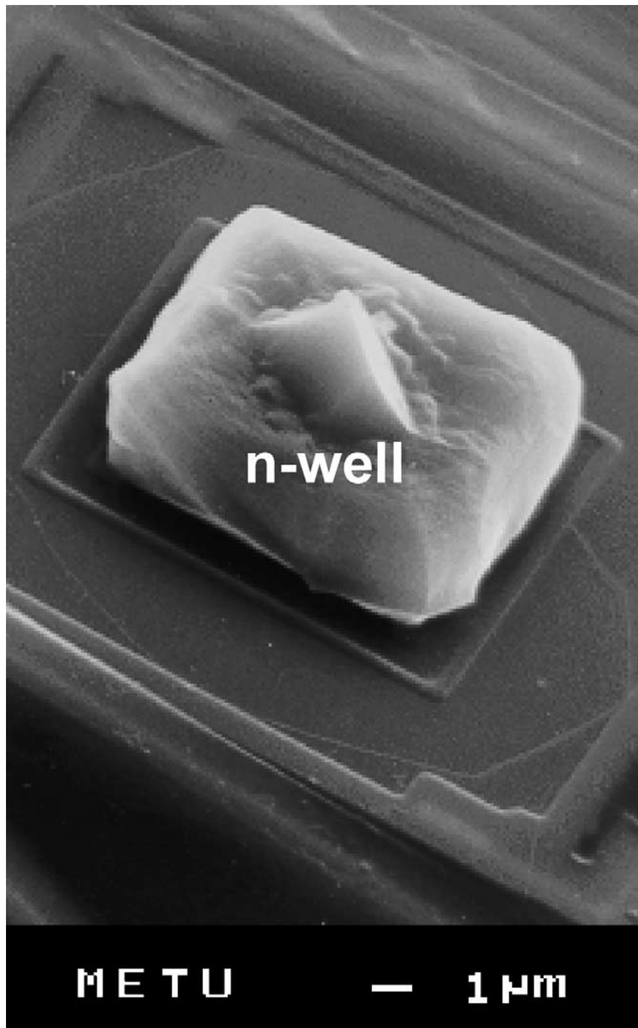

Fig. 4. The SEM photograph of the diode type detector taken looking from the backside, where the suspended n-well is clearly visible.

noise, noise equivalent temperature difference (NETD), detectivity (D^*), and self-heating.

3.1. Pixel size

The resistive type microbolometer detector is fabricated in a 0.8 μm CMOS process, and it has a pixel size of 80 μm × 80 μm with a fill factor of 13%. The pixel size cannot be decreased lower than a certain size determined by process design rules. For example, as a design rule constraint, the openings cannot be made narrower than 10 μm if post-CMOS bulk-micromachining is to be used. Another limitation for the pixel size reduction is the fact that the active pixel area cannot be made smaller than a certain size, since the resistance of the n-well layer should be much higher than the interconnect resistance to achieve better responsivity. In order to implement smaller pixels with higher fill factor, a sub-micron 0.35 μm CMOS process is used for the fabrication of new detectors. Considering the active area limitation of the resistive microbolometers, p^+-active/n-well diodes are used instead of n-well resistors to provide sufficient responsivity even at reduced pixel sizes. In order to reduce the opening widths, an RIE-based post-CMOS processing method is used, which also does not require any lithography step. With this new method, it is possible to define openings as narrow as 1.2 μm, allowing to reduce the pixel size to 40 μm × 40 μm while achieving an increased fill factor of 44%. Despite its reduced pixel size, the new diode type detector can still provide comparable or even better performance, while operating at a very low biasing level that also reduces self-heating.

3.2. Thermal conductance

Thermal isolation of a microbolometer detector from the substrate and its surrounding is the most important issue in the uncooled detector design. To achieve good thermal isolation n-well resistive and diode type microbolometers are operated in vacuum as other uncooled microbolometer detectors. Furthermore, thermal isolation also strongly depends on the interconnect material that provides electrical connection to the suspended microbolometer detector. The thermal isolation of the detector from the substrate can be improved by using polysilicon instead of metal interconnects on the support arms [16], at the expense of increased detector noise and reduced sensitivity. The thermal isolation is further improved by using longer L-shaped support arms in these small pixel structures.

Fig. 5(a) and (b) show the thermal simulation results obtained using the CoventorWare simulation tool for the resistive and p^+-active/n-well diode type microbolometers, respectively. In these simulations, constant power of 100 nW is assumed to be absorbed by the detector core, and the temperature gradient in the pixel is simulated in vacuum condition with respect to a reference temperature of 300 K. Using the applied power and corresponding temperature rise in the pixel, the thermal conductance and time constant of the resistive type microbolometer are determined as 6.7×10^{-7} W/K and 14 ms, respectively. The thermal conductance and thermal time constant for the diode type pixel are determined as 1.6×10^{-7} W/K and 27 ms, respectively.

Thermal conductance of the pixels is measured using self-heating effect: the pixel's temperature rises due to the joule-heating when it is biased in vacuum, and the pixel cools down to the ambient temperature when there is no bias. The change in the detector voltage is inversely proportional to the thermal conductance value, and it is directly proportional to the applied electrical power and temperature coefficient of pixel voltage or pixel resistance. Since the required bias current is very low for the diode detectors, most of the applied power is dissipated by the diode in the suspended n-well structure. In contrary, the required bias current is high for the resistive pixels, and therefore, power dissipated on the polysilicon interconnects is not negligible. Hence, temperature rise in the suspended pixel is less than one would expect when assuming that all the electrical power is dissipated in

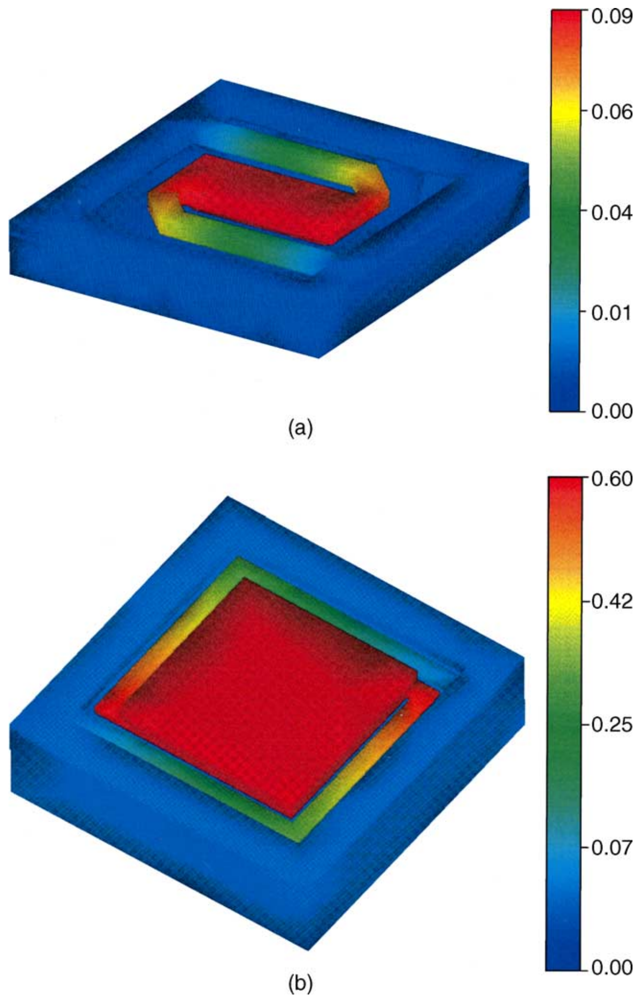

Fig. 5. The thermal simulation result obtained using the CoventorWare simulation tool; (a) for the resistive and (b) for the p^+-active/n^--well diode type microbolometers. In these simulations, constant power of 100 nW is assumed to be absorbed by the detector core, and the temperature gradient in the pixel is simulated in vacuum condition with respect to a reference temperature of 300 K.

the suspended detector structure, requiring a detailed analysis for the calculation of the detector's thermal conductance.

Fig. 6 shows the distributed thermal model of the pixel used in the analysis of the self-heating upon applied bias. In this model, the suspended structure is assumed to be a point detector with thermal conductance of G_{th}, and each support arm is divided into N units with thermal conductance values of $NG_{th}/2$. The temperature rise of the suspended n-well with respect to substrate, $\Delta T_{n\text{-well}}$, can be found by using superposition of individual power sources in the distributed model, which is given by,

$$\Delta T_{n\text{-well}} = \frac{P_{n\text{-well}}}{G_{th}} + 2\frac{P_{connect}}{NG_{th}}\sum_{k=1}^{N}\left[\frac{k}{N}\left\|\left(2-\frac{k}{N}\right)\right]\right. \times \frac{1}{(2-k/N)} \quad (1)$$

where, $P_{n\text{-well}}$ is the power dissipated in the suspended n-well and $P_{connect}$ is the power dissipated by the interconnect resistances on the support arms. After the series summation, the temperature rise reduces to,

$$\Delta T_{n\text{-well}} = \frac{P_{n\text{-well}}}{G_{th}} + \frac{P_{connect}N(N+1)}{2G_{th}N^2} \quad (2)$$

In the limit, when N goes to infinity, the result can be simplified as,

$$\lim_{N\to\infty}\Delta T_{n\text{-well}} = \frac{P_{n\text{-well}}}{G_{th}} + \frac{P_{connect}}{2G_{th}} \quad (3)$$

This result indicates that effective thermal conductance for the support arms actually doubles, decreasing the temperature rise upon applied bias. In the resistive pixel, $P_{connect}$ may be as high as $P_{n\text{-well}}$, therefore, pixel temperature rise is about 25% less than one would expect by assuming that all the pixel power is dissipated in the suspended n-well.

For the resistive pixels, the rise in the detector temperature results in a proportional increase in the detector resistance value related to its effective TCR value. Therefore, temperature rise in the detector can be found by measuring the change in detector resistance. Thermal conductance (G_{th}) can be extracted by calculating the power dissipated by the suspended n-well and interconnect resistors and using the temperature rise in the pixel. With this method, thermal conductance of the resistive pixels is measured as 6.2×10^{-7} W/K [17].

For the diode type pixels, the rise in detector temperature results in a proportional decrease in the detector voltage, related to the temperature coefficient of diode forward voltage and TCR of the interconnect resistance. Since the diode forward voltage has a strong temperature dependency, it is difficult to determine voltage and power distribution among the

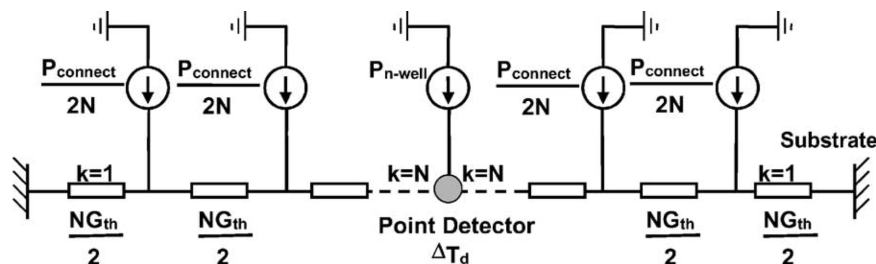

Fig. 6. The distributed thermal model of the pixel used in the analysis of self-heating of the pixel upon applied bias.

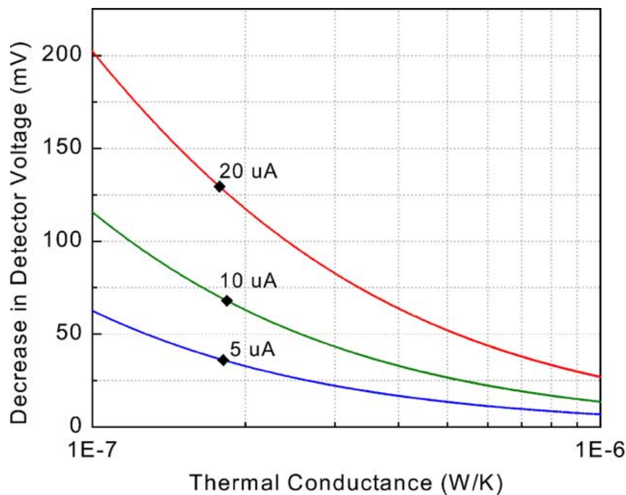

Fig. 7. The decrease in the detector voltage for different thermal conductance values ranging from 1.0×10^{-7} to 1.0×10^{-6} W/K simulated at three different bias levels of 5, 10, and 20 μA. Measurement results are marked on corresponding graphs.

n-well diode and interconnect resistance. In order to be able to determine the thermal conductance properly, self-heating and corresponding decrease in detector voltage have been simulated with respect to thermal conductance values at different bias levels. Fig. 7 shows the decrease in the detector voltage for different thermal conductance values ranging from 1.0×10^{-7} to 1.0×10^{-6} W/K simulated at three different bias levels of 5, 10, and 20 μA. The decrease in the detector voltage has been measured for the same bias levels at 80 mTorr, and the data are marked on corresponding graphs. The thermal conductance of the detector is found by averaging the corresponding thermal conductance values of each individual data point as 1.8×10^{-7} W/K. This measured value is in accordance with the simulated values during the design of the detector, where it is determined as 1.4×10^{-7} W/K according to the analytical calculations in MATLAB and 1.6×10^{-7} W/K according to the finite element simulation results in CoventorWare.

3.3. TCR and temperature coefficient of detector voltage

The effective TCR of the resistive type detector is the weighted average of the n-well and interconnect TCR values, which is given by,

$$\alpha_{\text{detector}} = \frac{R_{\text{n-well}}\alpha_{\text{n-well}} + R_{\text{connect}}\alpha_{\text{connect}}}{R_{\text{n-well}} + R_{\text{connect}}} \quad (4)$$

where, $R_{\text{n-well}}$ is the n-well resistance, R_{connect} is total interconnect resistance, and $\alpha_{\text{n-well}}$ and α_{connect} are corresponding TCR values of n-well and interconnect resistances, respectively. The measured effective TCR of the resistive pixel is 0.34%/K, which is smaller than the measured n-well TCR (0.65%/K), due to the low TCR of the polysilicon interconnect (0.1%/K) [17].

The effect of interconnect TCR is negligible in the diode type detectors, as the required bias current is low; therefore, the temperature sensitivity of the diode type detector is mainly determined by the temperature sensitivity of the diode forward voltage. The temperature sensitivity of the diode type detector voltage, dV_{det}/dT, at constant current bias is given by,

$$\frac{dV_{\text{det}}}{dT} = \frac{dV_{\text{D}}}{dT} + R_{\text{connect}} I_{\text{bias}} \alpha_{\text{connect}} \quad (5)$$

where, dV_{D}/dT is the temperature coefficient of diode forward voltage, R_{connect} is the interconnect resistance, I_{bias} is the detector bias current, and α_{connect} is the interconnect TCR values. Temperature coefficient of diode forward voltage is given by [14],

$$\frac{dV_{\text{D}}}{dT} = -\frac{n(1.21V - V_{\text{D}}/n)}{T} \quad (6)$$

where V_{D} is diode forward voltage, n is the junction voltage coefficient (close to unity), and T is temperature in Kelvin (K). The voltage, 1.21 V, is approximately constant for diode type detectors.

Diode forward voltage increases with increasing bias current, and hence its temperature sensitivity decreases in magnitude. Fig. 8 shows the simulated variation in the magnitude of detector voltage temperature sensitivity, $|dV_{\text{det}}/dT|$, with pixel bias current, I_{bias}. The magnitude of temperature sensitivity decreases from 2.35 to 1.65 mV/K when the bias current is increased from 1 to 100 μA. This result has been verified experimentally by measuring the sensitivities at different bias levels. Fig. 9 shows the measured variation of detector voltage, V_{det}, with temperature at different bias levels. Magnitude of the detector temperature sensitivity, $|dV_{\text{det}}/dT|$, is measured as 2.0 mV/K at 20 μA, and it

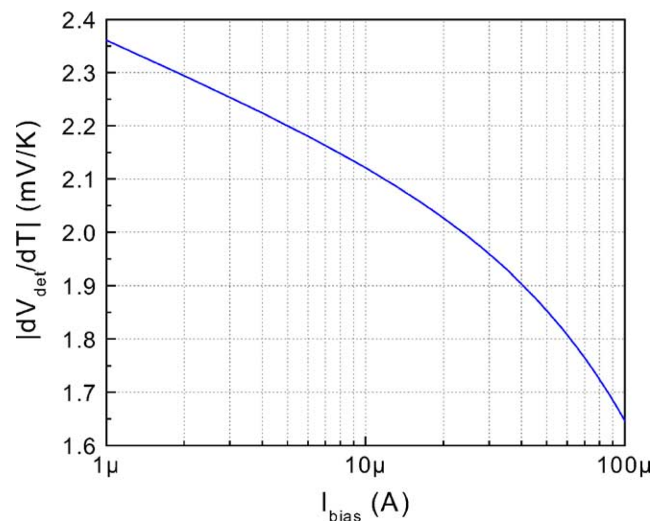

Fig. 8. The simulated variation in the magnitude of detector voltage temperature sensitivity, $|dV_{\text{det}}/dT|$, with pixel bias current, I_{bias}. The magnitude of temperature sensitivity decreases from 2.35 to 1.65 mV/K when the bias current is increased from 1 to 100 μA.

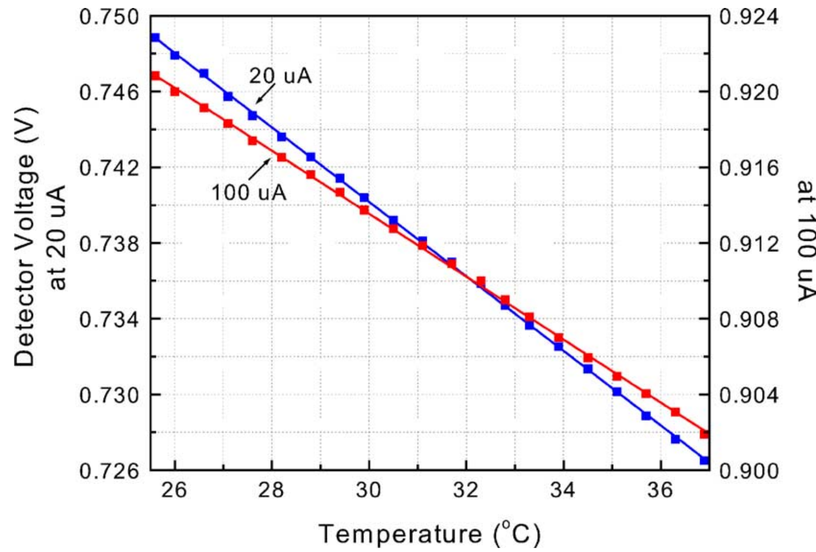

Fig. 9. The measured variation of detector voltage, V_{det}, with temperature at different bias levels. Magnitude of the detector temperature sensitivity, $|dV_{det}/dT|$, is measured as 2.0 mV/K at 20 μA, and it decreases to 1.7 mV/K at 100 μA, which is in accordance with the simulation results.

decreases to 1.7 mV/K at 100 μA, which is in accordance with the simulation results.

It should be noted here that the TCR expression of the resistive type detector in Eq. (4) and voltage temperature sensitivity expression of the diode type detector in Eq. (5) are given assuming that both the n-well and interconnects are at the same temperature. However, in the actual operation in vacuum, there is a temperature gradient between the suspended n-well and the substrate along the support arms. This temperature gradient reduces the effective TCR of the interconnect material to the half of its actual value. This effect should be considered in the responsivity expressions, as provided in the next section.

3.4. Responsivity

Fig. 10(a) and (b) show the simple models used in the derivation of the responsivity expressions for the resistive and diode type microbolometer detectors, respectively. For a fair comparison, bias current of the resistive detector is chosen in such a way that both type of detector provide the same NETD value. The dc responsivity of the resistive type microbolometer biased at constant current is given as,

$$\Re = \frac{\eta I_{bias} R_{det}}{G_{th}} \left(\frac{R_{n\text{-well}}\alpha_{n\text{-well}} + 0.5 R_{connect}\alpha_{connect}}{R_{det}} \right) \quad (7)$$

where η is the absorption coefficient, G_{th} is the detector thermal conductance, I_{bias} is the detector dc bias current, R_{det} is the total detector resistance, $R_{connect}$ is the interconnect resistance, $R_{n\text{-well}}$ is the n-well resistance, and $\alpha_{connect}$ and $\alpha_{n\text{-well}}$ are the TCR of the interconnect and n-well, respectively. In this expression, the term in parenthesis represents the effective TCR of the detector, which includes a factor of 0.5 in the numerator in front of $R_{connect}\alpha_{connect}$ term, different than the TCR expression given by Eq. (4). As mentioned previously, this is necessary to include the effect of temperature gradient along the interconnect resistor on the support arms. The dc responsivity of the diode type detector is given by,

$$\Re = \frac{\eta}{G_{th}} \left(-\frac{dV_D}{dT} - \frac{I_{bias} R_{connect}\alpha_{connect}}{2} \right) \quad (8)$$

where η, G_{th}, dV_D/dT, I_{bias}, $R_{connect}$, and $\alpha_{connect}$ are the absorption coefficient, thermal conductance, temperature coefficient of diode forward voltage, dc bias current, interconnect resistance, and interconnect TCR values, respectively. Similar to the resistive case, the term in the brackets represents the effective temperature coefficient of the detector voltage, which has a factor of 2 in the denominator of the last term to include the effect of temperature gradient along the interconnect resistor on the support arms.

It should be noted that the responsivity equations given in Eqs. (7) and (8) provide the dc responsivity, and the actual responsivity is lower than this dc responsivity value when the detectors are scanned at a certain rate. For example, when the detectors are scanned at 30 frames per second (fps), only 80 and 60% of the maximum output signal will be available at the end of the first period for the resistive and

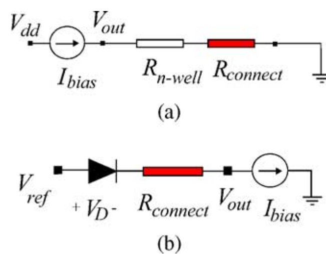

Fig. 10. The simple models used in the derivation of the responsivity expressions for the (a) resistive and (b) diode type microbolometers.

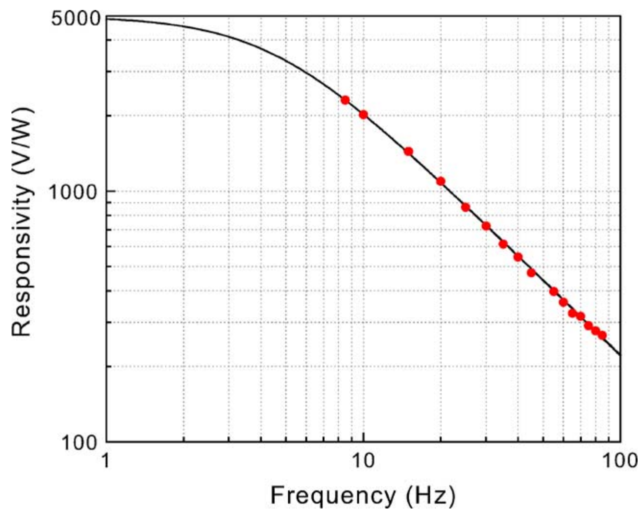

Fig. 11. The measured responsivity variation of the diode type detector with respect to chopper frequency from 8.5 to 85 Hz measured at 80 mTorr. The measurement result is fitted to a single-pole frequency response, and the dc responsivity and thermal time constant of the detector are extracted as 4970 V/W and 35.8 ms, respectively.

diode type detectors, respectively, due to their large thermal time constants. The dc responsivity and the thermal time constant of the detector can be measured by determining the detector responsivity with respect to the infrared radiation power modulated with a chopper.

Fig. 11 shows the measured responsivity variation of the diode type detector with respect to chopper frequency from 8.5 to 85 Hz measured at 80 mTorr. The measurement result is fitted to a single-pole frequency response, and the dc responsivity and thermal time constant of the detector are extracted as 4970 V/W and 35.8 ms, respectively. The absorption coefficient is extracted as 0.45 by plugging the measured responsivity value in the theoretical expression given in Eq. (8). This value is less than that of the resistive type detector (0.60) due to the reduced oxide thickness on top of the sensitive detector area. This reduction causes also a proportional loss in the responsivity and detectivity of the diode type pixels.

3.5. Electrical noise

Electrical noise of microbolometers is an important parameter that determines the minimum detectable level of infrared radiation, and it has several components. The noise in the n-well resistive detector principally consists of thermal (Johnson) noise and 1/*f* noise. Since the n-well layer is single-crystal, its 1/*f* noise is negligible, as verified with measured results given later. The diode type detectors also have low 1/*f* noise, as the bias current is low. This is a major advantage of n-well microbolometers over other microbolometers implemented with amorphous material where 1/*f* noise is considerably high.

Fig. 12(a) and (b) show the noise models of the resistive and diode type microbolometer detectors, respectively. The

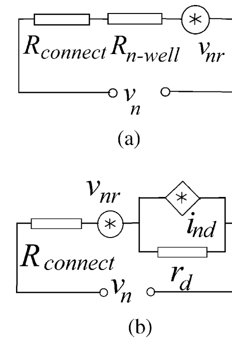

Fig. 12. The noise models of the (a) resistive and (b) diode type microbolometer detectors.

electrical noise power is composed of two parts: noise of the sensitive part and noise of the electrical interconnects. In the resistive case, both noise sources are coming from resistors, and the detector noise models is the series combination of the n-well and interconnect resistors. Since the 1/*f* noise is negligible, especially at low bias levels, the noise voltage can be expressed in the well-known thermal noise formula given by [24],

$$v_n = \sqrt{4\,kTR_{det}\,\Delta f} \quad (9)$$

where k is the Boltzmann constant, T is the temperature in Kelvin, R_{det} is the total detector resistance, and Δf is the electrical bandwidth.

In the diode case, the electrical noise of the detector is composed of two noise sources: noise of the interconnect resistor and noise of the p$^+$-active/n-well diode. The 1/*f* noise of the diode and polysilicon interconnects can be neglected due to their low values at low bias levels. Therefore, only the shot noise of the diode and the thermal noise of interconnect layers are considered in the calculation of detector noise. Total detector noise can be combined in an expression similar to the thermal noise expression of resistors by including the diode shot noise in terms of its dynamic resistance (r_d), which is given by [19],

$$v_n = \sqrt{4kT(R_{connect} + \tfrac{1}{2}r_d)\Delta f} \quad (10)$$

where $R_{connect}$ is the interconnect resistance and r_d is the dynamic resistance of the diode. This equation suggests that diode dynamic resistance should be decreased by increasing detector bias level in order to decrease the total noise of the pixel.

Fig. 13 shows the simulated variation of noise components for the diode type microbolometer coming from the p$^+$-active/n-well diode and interconnect resistance. As bias level is increased, dynamic resistance of the diode decreases inversely proportional to the bias current, therefore, the diode noise voltage decreases. Hence, the total detector noise approaches to that of the resistor thermal noise, as the bias level increases. Although it seems advantageous to operate the pixel at higher bias levels to achieve low noise, increasing bias current also decreases the responsivity as

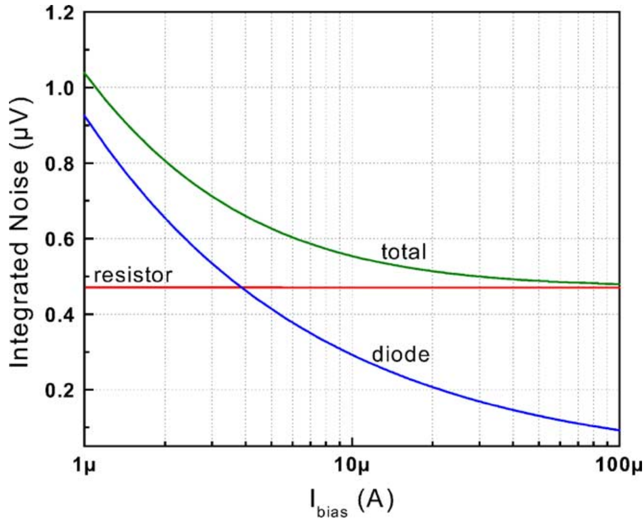

Fig. 13. The simulated variation of noise components for the diode type microbolometer coming from the p^+-active/n-well diode and interconnect resistance.

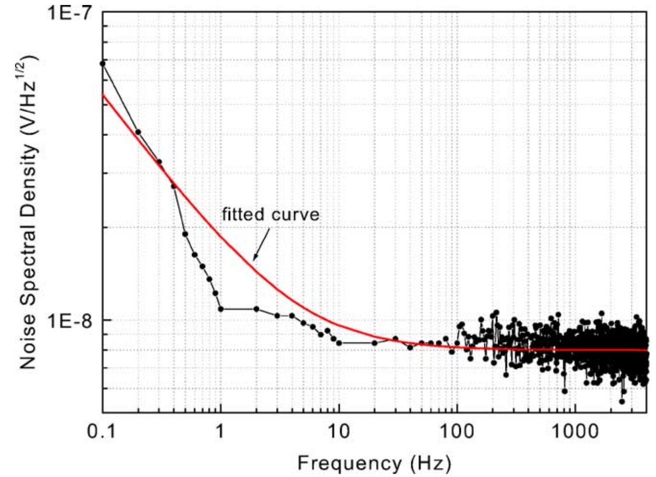

Fig. 15. The measured noise spectral density of the diode type microbolometers measured from 0.1 Hz to 4 kHz at 20 μA bias level. Using the asymptotic portion of the fitted curve in the low frequency region, the 1/*f* corner frequency is found as 4.4 Hz. Total rms noise voltage from 0.1 Hz to 4 kHz is measured as 0.52 μV.

explained before. Therefore, there is an optimum detectivity value achieved at a certain bias level, which is found to be 20 μA.

Fig. 14 shows the measured noise spectral density of a resistive type detector with 10 kΩ resistance value. The total rms noise voltage is measured as 0.81 μV in the 10–4000 Hz bandwidth, with an average noise spectral density of 12.8 nV/Hz$^{1/2}$ over the same bandwidth. The measured noise spectral density is very close to the thermal noise component (12.6 nV/Hz$^{1/2}$), verifying the fact that 1/*f* noise is low in the resistive n-well type detectors.

Fig. 15 shows the measured noise spectral density of the diode type microbolometers measured from 0.1 Hz to 4 kHz at a 20 μA bias level. The measured noise spectral density is fitted to an equation including 1/*f* noise and thermal noise components, which is given as,

$$v_n^2(f) = \frac{K}{f} + v_0^2 \quad (11)$$

where K and v_0 are 1/*f* noise coefficient and white noise component of the detector noise, respectively. From the fitted curve, K and v_0 are found as 2.84×10^{-16} V^2/Hz and 7.99 nV/Hz$^{1/2}$. Using the asymptotic portion of the fitted curve in the low frequency region, the 1/*f* corner frequency is found as 4.4 Hz. Total rms noise voltage from 0.1 Hz to 4 kHz is measured as 0.52 μV, which is very close to the calculated noise value, verifying that 1/*f* noise component can be neglected due to the single-crystal nature of the n-well and low level biasing.

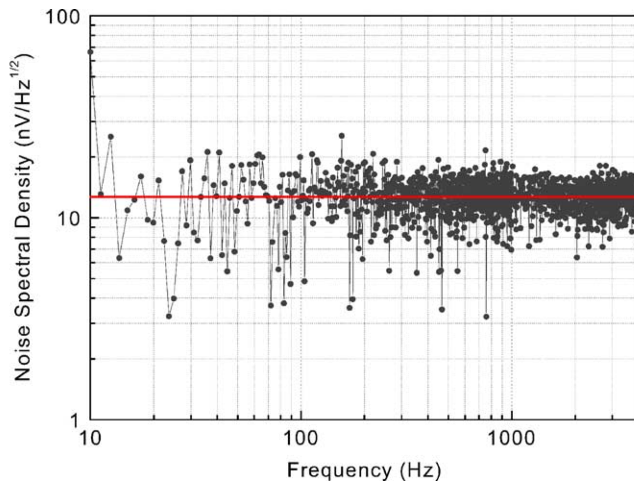

Fig. 14. The measured noise spectral density of a resistive type detector with 10 kΩ resistance value. Total rms noise voltage is measured as 0.81 μV in the 10–4000 Hz bandwidth, with an average noise spectral density of 12.8 nV/Hz$^{1/2}$ over the same bandwidth.

3.6. Noise equivalent temperature difference (NETD) and detectivity (D^*)

Noise equivalent temperature difference, and detectivity, D^*, are two important performance parameters for the infrared detectors, and they depend on biasing conditions. NETD value of the uncooled detectors can be defined as the change in the temperature of a blackbody that results in the signal to noise ratio of unity in the detector output signal [25]. NETD value depends both on the detector parameters and the optics used in infrared detection. The lower is the NETD value, the better is the detector performance. D^* is a normalized figure of merit which is used to compare different types of infrared detectors, and a high D^* value indicates a high detector performance. NETD and D^* values are defined as [25],

$$\text{NETD} = \frac{(4(f/D)^2 + 1)V_n}{A_D \Re (\Delta P/\Delta T)_{\lambda_1 - \lambda_2}} \quad (12)$$

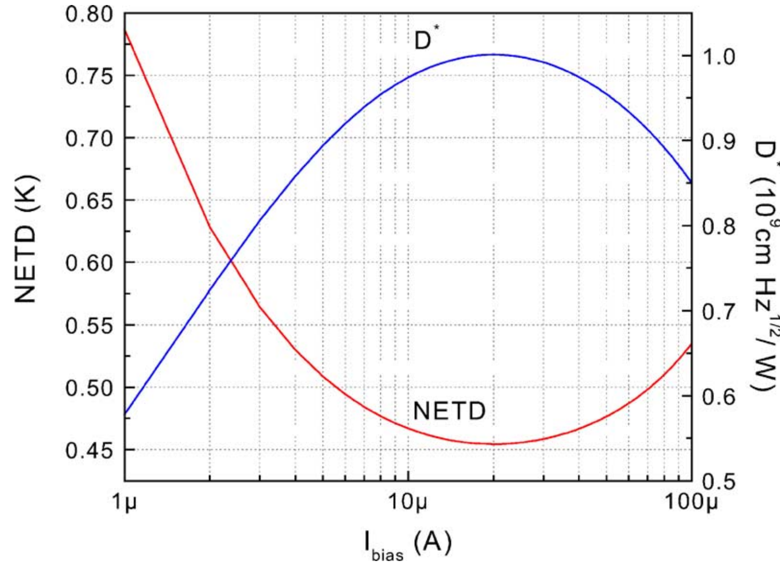

Fig. 16. The simulated variation of NETD and D^* values of the diode type pixel at different bias levels. At the optimum bias point of 20 μA, the diode type detector provides a measured D^* value of 9.7×10^8 cm $Hz^{1/2}$/W and an estimated NETD value of 470 mK for *f*/1 optics and 4 kHz electrical bandwidth.

$$D^* = \frac{\Re\sqrt{A_D \Delta f}}{V_n} \tag{13}$$

where *f* and *D* are the focal length and diameter of the optics, V_n is the total integrated noise voltage in the given electrical bandwidth of Δf, A_D is the active detector area, $\Re$ is the responsivity, and $(\Delta P/\Delta T)_{\lambda_1-\lambda_2}$ is a constant depending on the spectral band and is equal to 2.62×10^{-4} W/(cm^2 K) for the infrared detectors working in the 8–12 μm spectral window [25]. Fig. 16 shows the simulated variation of NETD and D^* values of the diode type pixel at different bias levels. Optimum performance is achieved at a 20 μA bias level, where total rms noise voltage is calculated as 0.52 μV for a 4 kHz electrical bandwidth. Noise power contributions of the interconnect resistor and diode are 85 and 15%, respectively [19]. At the optimum bias point of 20 μA, the diode type detector provides a measured D^* value of 9.7×10^8 cm $Hz^{1/2}$/W and an estimated NETD value of 470 mK for *f*/1 optics and 4 kHz electrical bandwidth. Note that this electrical bandwidth together with parallel readout circuitry is sufficient for the scanning of large format arrays, such as 128 × 128.

The resistive detector achieves the same estimated NETD value of 470 mK at about 170 μA, where it provides a D^* value of 8.9×10^8 cm $Hz^{1/2}$/W. It is possible to improve the performance values of the resistive detectors by increasing the bias level, since the signal-to-noise ratio of the detector output improves at higher bias levels; however, high bias levels increase self-heating as analyzed below.

3.7. Self-heating

Self-heating of the uncooled detectors is an important parameter affecting the operation of the readout circuit. Self-heating increases with the increasing bias level, and it should be reduced in order to avoid possible saturation problems of the readout circuit. Therefore, self-heating and bias levels of the detectors should be considered while comparing the NETD values of different detectors.

Fig. 17 shows the simulated variation of self-heating and NETD of both types of pixels with respect to bias current. For the resistive microbolometer, the NETD value decreases as the bias level increases. However, this results in an excessive self-heating problem that may be difficult to compensate for. Whereas, the diode type microbolometer can provide same NETD values at much lower bias levels with much less self-heating.

Table 1 gives the comparison summary for the resistive and diode type microbolometer detectors. At the optimum bias level of 20 μA, the diode type microbolometer detector

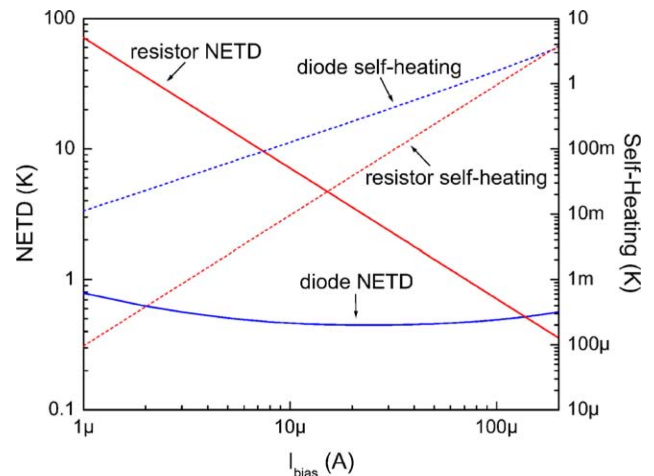

Fig. 17. The simulated variation of self-heating and NETD of both types of pixels with respect to bias current.

Table 1
The comparison summary for the resistive and diode type microbolometer detectors

Detector type	Resistor	Diode
CMOS process	AMS 0.8 μm	AMS 0.35 μm
Post-CMOS	Wet etch	RIE + wet etch
Pixel size (μm^2)	80 × 80	40 × 40
Fill factor (%)	13	44
G_{th} (W/K)	6.2×10^{-7}	1.8×10^{-7}
Absorption coefficient	0.6	0.45
Time constant (ms)	21	35.8
I_{bias} (μA)	170	20
Self-heating (K)	2.7	0.27
Electrical noise (μV)	0.81	0.52
Sensitivity	0.34%/K	−2.0 mV/K
The dc responsivity (V/W)	4970	4970
NETD (mK) (*f*/1)	470[a]	470[a]
D^* (cm Hz$^{1/2}$/W)	8.9×10^8	9.7×10^8

[a] Expected.

has a dc responsivity ($\mathfrak{R}$) value of 4970 V/W. Corresponding NETD and detectivity (D^*) values are 470 mK and 9.7×10^8 cm Hz$^{1/2}$/W, respectively. At a 20 μA bias with 125 μsec pulse duration, the diode type microbolometer has a self-heating of 0.27 K. The resistive type microbolometer requires about 8 times higher bias current to obtain the same NETD value as the diode type detector, resulting in an excessive self-heating of 2.7 K, which is 10 times larger as compared to that of the diode type detector.

4. Conclusions

This paper reports the implementation and comparison of two low-cost uncooled infrared microbolometer detectors that can be implemented using standard n-well CMOS processes: n-well resistive and p^+-active/n-well diode detectors. The resistive n-well detector is implemented in a 0.8 μm CMOS process and has a pixel size of 80 μm × 80 μm with a fill factor of 13%. The diode type detector is implemented in a sub-micron 0.35 μm CMOS process and has a pixel size of 40 μm × 40 μm with a fill factor of 44%. These detectors can be obtained with simple bulk-micromachining processes after the CMOS fabrication, without the need for any complicated lithography or deposition steps. Therefore, the detector cost is almost equal to the CMOS chip cost. The p^+-active/n-well diode detector has a measured dc responsivity ($\mathfrak{R}$) and detectivity (D^*) values of 4970 V/W and 9.7×10^8 cm Hz$^{1/2}$/W, respectively. The diode type detector has an estimated NETD value of 470 mK with an *f*/1 optics and 4 kHz electrical bandwidth. The resistive type n-well detector provides the same NETD value of 470 mK at 1.68 V detector bias voltage, where a self-heating of 2.7 K occurs. This self-heating is 10 times larger than that of the diode type detector and complicates the readout circuit. The performance of the resistive detector can be improved further with higher detector bias voltages; however, this increases the self-heating further. These results show that the diode type microbolometer detector is much more suitable for uncooled infrared imagers with large format arrays due to its small pixel size, low bias requirements, and reduced self-heating.

Acknowledgements

This work is initially sponsored by NATO's Scientific Affairs Division in the framework of the Science for Stability Program. This work is partially sponsored by ASELSAN Inc. and Research and Development Department of Ministry of Defense (MSB ArGe). The authors would like to thank Mr. Orhan Akar for his help in detector fabrication. The authors would also like to thank Prof. Dr. Ekmel Ozbay and Mr. Murat Gure from Physics Department of Bilkent University for their collaboration and help in dry etching steps, and Prof. Dr. Bilgehan Ogel and Mr. Cengiz Tan from Metallurgical Engineering Department of METU for their help in SEM photography.

References

[1] D. Murphy, M. Ray, R. Wyles, J. Asbrock, N. Lum, J. Wyles, C. Hewitt, G. Graham, W. Radford, J. Anderson, D. Bradley, R. Chin, T. Kostrzewa, High sensitivity (25 μm pitch) microbolometer FPAs and application development, Infrared Technology and Applications XXVII, Orlando, USA, 16–20 April, Proc. SPIE 4369 (2001) 222–234.

[2] R.A. Wood, Uncooled thermal imaging with monolithic silicon focal planes, Infrared Technology XIX, Proc. SPIE 2020 (1993) 322–329.

[3] E. Mottin, J. Martin, J. Ouvrier-Buffet, M. Vilain, A. Bain, J. Yon, J.L. Tissot, J.P. Chatard, Enhanced amorphous silicon technology for 320 × 240 microbolometer arrays with a pitch of 35 μm, Infrared Technology and Applications XXVII, Orlando, USA, 16–20 April, Proc. SPIE 4369 (2001) 250–256.

[4] T. Ichihara, Y. Watabe, Y. Honda, K. Aizawa, A high performance amorphous $Si_{1-x}C_x$:H thermistor bolometer based on micromachined structure, in: Presented at International Conference on Solid−State Sensors and Actuators (TRANSDUCERS'97), Chicago, USA, 16–19 June 1997, pp. 1253–1256.

[5] S. Sedky, P. Fiorini, K. Baert, L. Hermans, R. Mertens, Characterization and optimization of infrared poly SiGe bolometers, IEEE Trans. Electron. Devices 46 (1999) 675–682.

[6] H. Wada, T. Sone, H. Hata, Y. Nakaki, O. Kaneda, Y. Ohta, M. Ueno, M. Kimata, YBaCuO uncooled microbolometer IR FPA, Infrared Technology and Applications XXVII, Orlando, USA, 16–20 April, Proc. SPIE 4369 (2001) 297–304.

[7] M. Almasri, D.P. Butler, Z.C. Butler, Semiconducting YBCO bolometers for uncooled IR detection, Infrared Detectors and Focal Plane Arrays VI, Orlando, USA, 24–28 April, Proc. SPIE 4028 (2000) 17–26.

[8] A. Tanaka, S. Matsumoto, N. Tsukamoto, S. Itoh, T. Endoh, A. Nakazato, Y. Kumazawa, M. Hijikawa, H. Gotoh, T. Tanaka, N. Teranishi, Silicon IC process compatible bolometer infrared focal plane array, in: Presented at the International Conference on Solid-State Sensors and Actuators (TRANSDUCERS'95), Stockholm, Sweden, 25–29 June 1995, pp. 632–635.

[9] H.-K. Lee, J.-B. Yoon, E. Yoon, S.-B. Ju, Y.-J. Yong, W. Lee, S.-G. Kim, A high fill−factor infrared bolometer using micromachined

multilevel electrothermal structures, IEEE Trans. Electron. Devices 46 (1999) 1489–1491.
[10] A.D. Oliver, K.D. Wise, A 1024-element bulk-micromachined thermopile infrared imaging array, Sens. Actuators A 73 (1999) 222–231.
[11] A. Schaufelbuhl, N. Schneeberger, U. Munch, M. Waelti, O. Paul, O. Brand, H. Baltes, C. Menolfi, Q. Huang, E. Doering, M. Loepfe, Uncooled low-cost thermal imager based on micromachined CMOS integrated sensor array, J. Microelectromech. Syst. 10 (2001) 503–510.
[12] J. Kim, C. Han, A new uncooled thermal infrared detector using silicon diode, Sens. Actuators A 89 (2001) 22–27.
[13] J.C. Brasunas, B. Lakew, R. Fettig, A comment on reported detectivity of a new uncooled thermal infrared detector, Sens. Actuators A 96 (2002) 211–213.
[14] T. Ishikawa, M. Ueno, Y. Nakaki, K. Endo, Y. Ohta, J. Nakanishi, Y. Kosasayama, H. Yagi, T. Sone, M. Kimata, Performance of 320 × 240 uncooled IRFPA with SOI diode detectors, Infrared Technology and Applications XXVI, San Diego, USA, 30 July–4 August, Proc. SPIE 4130 (2000) 1–8.
[15] S. Eminoglu, D.S. Tezcan, M.Y. Tanrikulu, T. Akin, Low-cost uncooled infrared detectors in CMOS process, in: Presented at the 16th European Conference on Solid-State Transducers (EUROSENSORS XVI), Prague, Czech Republic, 15–18 September 2002, pp. 263–264.
[16] D.S. Tezcan, F. Kocer, T. Akin, An uncooled microbolometer infrared detector in any standard CMOS technology, in: Presented at the International Conference on Solid-State Sensors and Actuators (TRANSDUCERS'99), Sendai, Japan, 7–10 June 1999, pp. 610–613.
[17] D.S. Tezcan, S. Eminoglu, O.S. Akar, T. Akin, A low cost uncooled infrared microbolometer focal plane array using the CMOS n-well layer, in: Presented at the 14th IEEE International Microelectromechanical Systems Conference (MEMS 2001), Interlaken, Switzerland, 21–25 January 2001, pp. 566–569.
[18] D.S. Tezcan, S. Eminoglu, O.S. Akar, T. Akin, An uncooled microbolometer infrared focal plane array in standard CMOS, Photodetector Materials and Devices VI, San Jose, USA, 20–26 January, Proc. SPIE 4288 (2001) 112–121.
[19] S. Eminoglu, M.Y. Tanrikulu, D.S. Tezcan, T. Akin, A Low-Cost, small pixel uncooled infrared detector for large focal plane arrays using a standard CMOS process, Infrared Detectors and Focal Plane Arrays VII, Orlando, USA, 1–5 April, Proc. SPIE 4721 (2002) 111–121.
[20] M. Parameswaran, H. Baltes, L. Ristic, D. Dhaded, A. Robinson, A new approach for the fabrication of micromechanical structures, Sens. Actuators A 19 (1989) 289–307.
[21] T. Akin, Z. Olgun, O. Akar, H. Kulah, An integrated thermopile structure with high responsivity using any standard CMOS process, Sens. Actuators A 66 (1998) 218–224.
[22] N. Schneeberger, O. Paul, H. Baltes, Spectral infrared absorption of CMOS thin film stacks, in: Presented at the International Conference on Microelectromechanical Systems (MEMS'99), Orlando, USA, 17–21 January 1999, pp. 106–111.
[23] G.K. Fedder, S. Santhanam, M.L. Reed, S.C. Eagle, D.F. Guillou, M.S.-C. Lu, L.R. Carley, Laminated high-aspect ratio microstructures in a conventional CMOS process, Sens. Actuators A 57 (1996) 103–110.
[24] B. Rezavi, Design of Analog CMOS Integrated Circuits, McGraw-Hill, New York, 2001.
[25] P.W. Kruse, Uncooled Thermal Imaging Arrays, Systems, and Applications, SPIE Press, 2001.

Biographies

Selim Eminoglu was born in Ankara, Turkey in 1973. He received his BS, MS, and PhD degrees in electrical engineering with honors from Middle East Technical University (METU), Ankara, in 1996, 1998, and 2003, respectively. His doctoral studies focused on the design and implementation of uncooled infrared focal plane arrays in CMOS technology. From 1995 to 1998, he has worked as a part-time researcher in the VLSI Design Center of TUBITAK–BILTEN where he has contributed to the development of a programmable mixed-signal ASIC chip for audio band signal processing applications. From 1996 to 2003, he was employed as a teaching and research assistant in the Electrical and Electronics Engineering Department of METU. Currently, he is working as a research scientist in the Rockwell Scientific Company, USA. His research interests include infrared detectors and readout circuits, and analog and digital integrated circuit design for signal processing applications.

Deniz Sabuncuoglu Tezcan was born in Ankara, Turkey, in 1973. She received her BS, MS, and PhD degrees in electrical engineering with honors from Middle East Technical University (METU), Ankara, in 1995, 1997, and 2002, respectively. Her doctoral studies focused on fabrication, modeling, and characterization of n-well microbolometer type uncooled infrared detectors implemented in CMOS technology. From 1995 to 2002, she was employed as a teaching and research assistant in the Electrical and Electronics Engineering Department of METU. From 2002 to 2003, she worked as an Instructor in the same department. From September 1998 to January 1999, she continued her studies in IMEC, Belgium through Integrated PhD Scholarship Program from the Scientific and Technical Research Council of Turkey (TUBITAK). Currently, she is pursuing her post-doctoral studies in IMES, Belgium.

M. Yusuf Tanrikulu was born in Tarsus, Turkey in 1978. He received his BS and MS degrees in electrical engineering with high honors from Middle East Technical University (METU), Ankara, in 2000 and 2002, respectively. His master studies focused on modeling, fabrication, and characterization of high fill factor microbolometer type uncooled infrared detectors implemented in CMOS technology. Currently he is pursuing his PhD degree in the Electrical and Electronics Engineering Department of METU on the design and implementation of uncooled infrared microbolometer arrays. Since 2000, he has been employed as a teaching and research assistant in the same department.

Tayfun Akin was born in Van, Turkey, in 1966. He received the BS degree in electrical engineering with high honors from Middle East Technical University, Ankara, in 1987 and went to the USA in 1987 for his graduate studies with a graduate fellowship provided by NATO Science Scholarship Program through the Scientific and Technical Research Council of Turkey (TUBITAK). He received the MS degree in 1989 and the PhD degree in 1994 in electrical engineering, both from the University of Michigan, Ann Arbor. Since 1995 and 1998, he has been employed as an Assistant Professor and Associate Professor, respectively, in the Department of Electrical and Electronics Engineering at Middle East Technical University, Ankara, Turkey. He is also the technical coordinator of METU-MET, an IC fabrication factory which is transferred to Middle East Technical University by the government for MEMS related production. His research interests include MEMS (micro-electro-mechanical systems), Microsystems Technologies, infrared detectors and readout circuits, silicon-based integrated sensors and transducers, and analog and digital integrated circuit design. He has served in various MEMS, EUROSENSORS, and TRANSDUCERS conferences as a Technical Program Committee Member. He is the designate co-chair of IEEE MEMS Conference to be held in 2006. He is the winner of the First Prize in Experienced Analog/Digital Mixed-Signal Design Category at the 1994 Student VLSI Circuit Design Contest organized and sponsored by Mentor Graphics, Texas Instruments, Hewlett-Packard, Sun Microsystems, and Electronic Design Magazine. He is the co-author of the symmetric and decoupled gyroscope project which won the first prize award in the operational designs category of the international design contest organized by DATE Conference and CMP in March 2001. He is also the co-author of the gyroscope project which won the third prize award of 3-D MEMS Design Challenge organized by "MEMGen Corp. (currently, Microfabrica)."